Nuclear Instruments and Methods in Physics Research B 365 (2015) 196–201

Contents lists available at ScienceDirect

Nuclear Instruments and Methods in Physics Research B

journal homepage: www.elsevier.com/locate/nimb

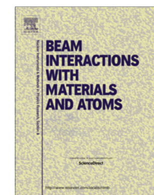

The effects of interfacial interactions between Fe–O and Fe–Si induced by ion-beam bombardment on the magnetic properties of Si-oxide/Fe bilayers

X. Li [a], K.-W. Lin [b,*], H.-T. Liang [b], H.-F. Hsu [b], N.G. Galkin [c], Y. Wroczynskyj [d], J. van Lierop [d,*], P.W.T. Pong [a,*]

[a] Department of Electrical and Electronic Engineering, The University of Hong Kong, Hong Kong
[b] Department of Materials Science and Engineering, National Chung Hsing University, Taichung 402, Taiwan
[c] Institute of Automation & Control Processes, FEB RAS, Radio Str. 5, 690041 Vladivostok, Russia
[d] Department of Physics and Astronomy, University of Manitoba, Winnipeg R3T 2N2, Canada

ARTICLE INFO

Article history:
Received 1 October 2014
Received in revised form 16 July 2015
Accepted 16 July 2015
Available online 3 August 2015

Keywords:
Ion-beam bombardment
Interface
Si-oxide/Fe bilayers
Thin film magnetism

ABSTRACT

Si/Fe and SiO_2/Fe thin-film heterostructures are commonly seen in magnetic multilayer devices, whose magnetic properties are strongly influenced by intermixing at the interfaces. In this paper, Si-oxide/Fe bilayers were formed by depositing Si on Fe with in situ O_2/Ar ion-beam bombardment during the Si deposition. The surface oxidation conditions were altered by applying different O_2/Ar ratios (0–41%) in the ion-beam. The surface and cross-sectional morphologies, and the crystalline structures were characterized by transmission electron microscopy. The formation of Fe–O, Fe–Si and Si–O bonds at the interface of the O_2/Ar ion-beam bombarded Si-oxide/Fe bilayers was evidenced by X-ray photoemission spectra. FeO, Fe_3O_4 and Fe_2O_3 at the interface resulted in a marked increase in the magnetic coercivity at low temperatures, as characterized by magnetometry.

© 2015 Elsevier B.V. All rights reserved.

1. Introduction

The properties of magnetic thin films have drawn great interest due in part to the surface and interface effects [1,2] that can be present. The structural [3,4], electrical [5] and magnetic [6] properties of Fe thin films with interfaces joined to other materials have been investigated intensively due to their potential applications in spintronic devices such as magnetic tunneling junctions [7]. One of the most widely investigated systems is the Fe/Si combination [8]. The magnetic anisotropy of Fe thin films deposited on Si (111) substrates could be tailored by changing the deposition incidence angle [9] and introducing a capping layer [10]. The formation of iron silicides at the interface can result in a drastic drop in the overall Fe layer magnetization [10]. The phases from intermixing at the interface of Si/Fe or Fe/Si are also inequivalent: it is ferromagnetic when depositing a Fe layer on Si [11], whereas it is nonmagnetic when a Fe layer is capped with Si [12]. The interface between SiO_2 and Fe, on the other hand, is more complex since it involves the formation of both silicide and Fe-oxides [13]. FeO and Fe_2O_3 are antiferromagnetic at low temperature and induce unusual hysteresis loop broadening and field shifts through exchange coupling with the ferromagnetic Fe [14,15]. These Fe-oxides could be formed either by reacting with the interfacing SiO_2 or with the residual oxygen in the coating chamber. Ti sublimation was introduced to reduce the amount of residual oxygen during the deposition of granular Fe-SiO_2 films, which resulted in fewer Fe-oxides and lower coercivity [16]. However, how the oxides influenced the microstructure and magnetic properties of Si-oxide/Fe bilayer thin films has not yet been reported. The evolution of the chemical composition at the interfaces of Si-oxide/Fe with increasing oxidation conditions remains unclear.

Ion-beam bombardment is commonly used in the preparation and investigation of magnetic thin films to alter the interface roughness [17], crystalline structures [18], domain structures [19], and to tailor the chemical composition [20]. The structural and compositional changes could be easily tailored by adjusting the ion-beam voltage [21] or reactive-gas content [22]. Post ion-beam bombardment was conducted on the Fe surface of Fe/Si [23,24] and Fe/SiO_2 [25,26] bilayers, and the ion mixing properties were reported. However, the in situ ion-beam bombardment,

* Corresponding authors. Tel.: +886 4 22851068, +1 (204) 474 6191, +852 2857 8491; fax: +886 4 22857017, +1 (204) 474 7622, +852 2559 8738.
E-mail addresses: kwlin@dragon.nchu.edu.tw (K.-W. Lin), johan@physics.umanitoba.ca (J. van Lierop), ppong@eee.hku.hk (P.W.T. Pong).

http://dx.doi.org/10.1016/j.nimb.2015.07.087
0168-583X/© 2015 Elsevier B.V. All rights reserved.

especially with a reactive gas during Si deposition, has yet to be reported for Si-oxide/Fe bilayers.

In this paper, ion-beam deposition was used to prepare Fe thin films with a Si or Si-oxide capping layer. The structure and composition of the capping layer was altered by ion-beam bombardment under different O_2/Ar ratios. The microstructure, chemical composition, and magnetic properties of Si/Fe and Si-oxide/Fe films were investigated to examine the effects of Fe–Si and Fe–O bonds and the results magnetism on the Fe layers capped with Si or Si-oxide. The comparison between the microstructures and magnetic properties in un-bombarded Si/Fe and Si-oxide (O_2/Ar)/Fe will further help reveal the intermixing and reaction produce effects on SiO_2/Fe thin film interfaces.

2. Experimental methods

25-nm Fe and 12-nm Si layers were deposited successively on thermally oxidized wafer substrates by dual-ion-beam sputtering deposition [27]. A Kaufman deposition source (V_K = 800 V) was engaged to sputter the Fe or Si targets. An End-Hall assist source (V_{EH} = 100 V) was operated with O_2/Ar ratios from 0% to 41% to in situ bombard the film during the deposition of Si layer. The surface and cross-sectional morphologies and the selected area electron diffraction (SAED) patterns of both ion-beam bombarded Si-oxide/Fe bilayers and the un-bombarded Si/Fe bilayer were characterized by a JEOL (JEM-2100F) high-resolution transmission electron microscope (HRTEM). The depth profile of the composition and bonding energy of Fe2p, Si2p and O1s of Si/Fe and Si-oxide (41% O_2/Ar)/Fe bilayers were characterized by a ULVAC-PHI (PHI 5000 Versa Probe) X-ray photoelectron spectrometer (XPS). The magnetic hysteresis loops of all the samples were measured by an ADE-DMS vibrating sample magnetometer (VSM) at room temperature and 180 K after cooling in 1.2 T field. In order to further investigate the magnetothermal properties, the samples were field-cooled in 5 T from 350 K to 10 K, and hysteresis loops were measured with a superconducting quantum interference device (SQUID) magnetometer (Quantum Design MPMS XL).

3. Results and discussions

The surface morphologies and SAED patterns of a Si single layer, an un-bombarded Si/Fe bilayer, and Si-oxide/Fe bilayers bombarded with O_2/Ar ratio ranging from 0% to 41% are presented in Fig. 1(a)–(f), respectively. The silicon single layers deposited on the substrate present an amorphous structure, which was evidenced by the broadened rings in SAED pattern (inset of Fig. 1(a)). All the Si/Fe and Si-oxide/Fe bilayers prepared in this experiment are polycrystalline, with grain sizes ranging from 5 to 15 nm. The surface morphologies were changed significantly by the ion-beam bombardment. Uniform surface phase structures with small grains were observed in bilayers bombarded with pure Ar (Fig. 1(c)) and 8% O_2/Ar (Fig. 1(d)). However, ion-beam bombardment with higher O_2/Ar ratio altered the compositions and preferred orientations of the surface Si-oxide layer, resulting in nonuniform crystalline phase structures and a wider distribution of grain sizes, as seen in the TEM images (Fig. 1(e) and (f)). The SAED patterns are labeled according to the corresponding interplane spacing. Since the diffraction rings are broadened and sometimes discrete, it is not likely that the corresponding lattices are highly ordered crystalline phases. It is more likely that a group of atoms formed ordered structure within a short range, thus having the corresponding interplane spacings. In the SAED patterns of the un-bombarded Si/Fe bilayer, diffraction rings of FeSi (1 1 1) (2 0 0) (4 2 1) and $FeSi_2$ (1 1 2) can be observed (Fig. 1(b) inset), indicating

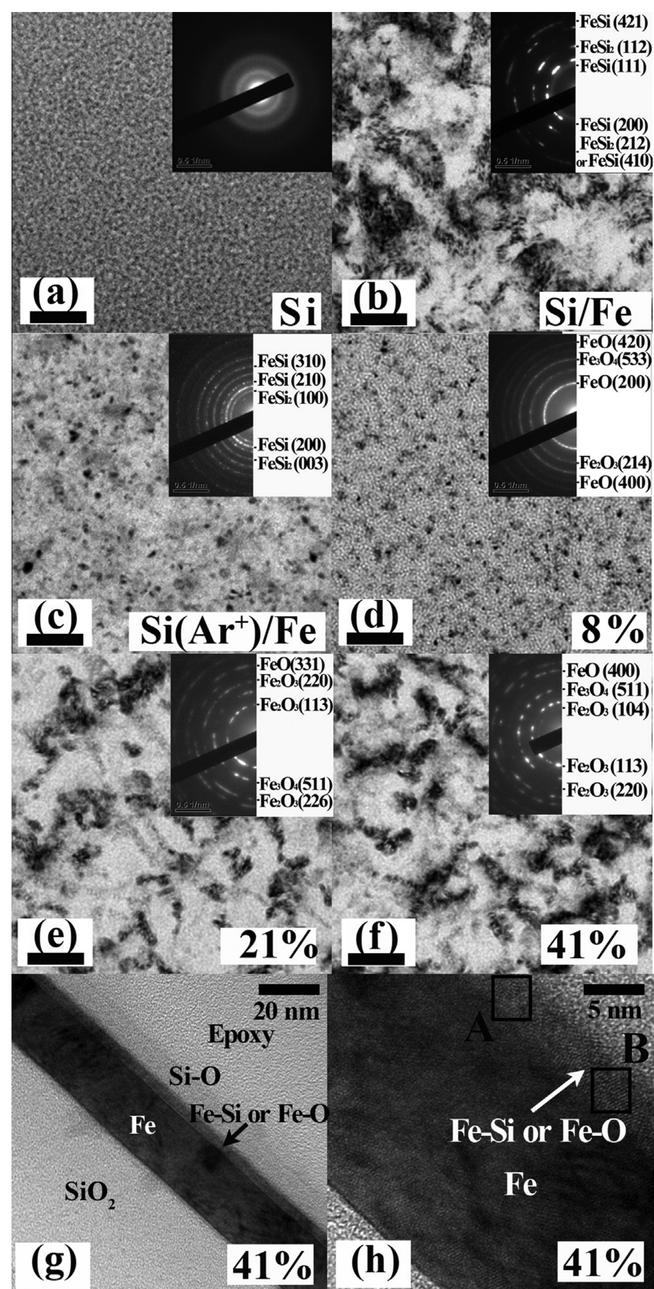

Fig. 1. The TEM characterization: The surface morphology (scale bar 40 nm) and SAED patterns of (a) Si single layer, (b) un-bombarded Si/Fe, (c) Ar^+ ion beam bombarded Si/Fe, (d) Si-oxide (8% O_2/Ar)/Fe, (e) Si-oxide (21% O_2/Ar)/Fe and (f) Si-oxide (41% O_2/Ar)/Fe bilayers, and (g) (h) the cross-sectional morphologies of Si-oxide (41% O_2/Ar)/Fe bilayer shown in different magnification.

the Si and Fe atoms formed bonds at the interface [8]. Ar^+ ion-beam bombardment altered the preferred orientation of the interfacial layer as indicated by the innermost diffraction ring of $FeSi_2$ (1 0 0) in the inset of Fig. 1(c). With oxygen in the ion beam, grains containing FeO, Fe_2O_3 and Fe_3O_4 (insets of Fig. 1(d)–(f)) were introduced. The electron diffraction pattern of the Si-oxide (8% O_2/Ar)/Fe bilayer is dominated by the Wustite FeO phase, including the planes of (2 0 0) (d = 0.15 nm), (4 0 0) (d = 0.107 nm), and (4 2 0) (d = 0.096 nm). With increasing oxygen content in the ion-beam, the FeO was further oxidized to Fe_3O_4 and Fe_2O_3, indicated by the emergence of the diffraction rings of the inverse spinels Fe_3O_4 (5 1 1) (d = 0.156 nm) and α-Fe_2O_3 (2 2 0) (d = 0.126 nm). This difference in the chemical composition was responsible for

the distinct differences in the microstructures observed in Fig. 1(d)–(f). In order to further investigate the crystalline structures of this sample, the cross-sectional morphologies of Si-oxide (41% O_2/Ar)/Fe bilayer were characterized by HRTEM. In Fig. 1(g), a clear interfacial layer could be observed between the Fe and Si-oxide layers. A closer view of the interfacial layer in Fig. 1(h) reveals the existence of both amorphous (region A) and crystalline phases (region B). The thickness of the interfacial layer (4 nm) is estimated to be comparable to the implantation depth of the Ar ions under 100 V ion-beam bombardment energy (e.g. the damage depth is 2–3 nm in Si substrates bombarded by 100 eV Ar ion-beam [28]). The amorphous phases are believed to be resulted from the ion-beam-bombardment-induced structural disorder. The crystalline lattices in region B of Fig. 1(h), on the other hand, are believed to be Fe–O grains, inferred from the SAED patterns in Fig. 1(f). The size of these grains is limited to several nanometers by the surrounding amorphous phases, presenting the character of short-range order. This is also consistent with the discrete electron diffraction rings in the inset of Fig. 1(f), which indicate that only small number of grains were included in the selected region.

In order to gain some quantitative information about the chemical composition in the bilayers, sputter etching was conducted on the sample surface, and XPS was performed after each etching stage. Fig. 2(a) shows the depth profiles of the relative atomic concentrations in the un-bombarded Si/Fe bilayer. The content of Si and Fe changes gradually at the interface, indicating the existence of strong Fe–Si intermixing with varying composition. The formation of iron silicide was evidenced by the shift in the peaks of the Fe2p (Fig. 2(b)) and Si2p (Fig. 2(c)) transitions in the XPS spectra. The binding energy for $Fe2p_{3/2}$ is 706.75 eV in bulk Fe [29], which is consistent with our result measured in the Fe layer (1.54-min sputtering in Fig. 2(b)). However, the peak shifted to 707.2 eV when measured at the Si/Fe interface (0.7-min sputtering in Fig. 2(b)), corresponds to the $Fe2p_{3/2}$ peak in FeSi or $FeSi_2$ [30]. This compositional change is also evidenced by the Si2p peak shift from 99.3 eV in the top Si layer (Fig. 2(c) 0.42 min) to 99.4 eV in the interface (Fig. 2(c) 0.7 min). After a 3.7-min sputter etching, the silicon dioxide on the substrate was detected, and the Si2p peak shifted to 104.4 eV. The content of oxygen in the Si/Fe interface is very low. The O1s peak at 533.2 eV indicated that oxygen atoms exist mainly in silicon oxides [31].

The composition of the Si-oxide (41% O_2/Ar)/Fe bilayer, on the other hand, is very different from that of the un-bombarded bilayers, as shown in Fig. 3(a). Due to the high O_2/Ar ratio, the Si in the capping layer was fully oxidized. The oxygen content in the surface Si-oxide layer is slightly higher than that in the thermally oxidized SiO_2 layer and the naturally oxidized SiO_2. Excess oxygen atoms may exist as iron oxides or in the interstices. This is also indicated by the change in the Si2p binding energy from 103.6 eV in the surface Si-oxide layer (Fig. 3(b) 0.14 min) to 104.3 eV in the thermal oxides (Fig. 3(b) 3.08 min). The ion-beam bombardment and interfacial intermixing also resulted in an interfacial layer between Si-oxide and Fe layers (marked as I in Fig. 3(a)), which is also observed in the HRTEM image in Fig. 1(h). Silicon oxides, iron oxides and iron silicide could be tracked. For example, an asymmetric $Fe2p_{3/2}$ peak was observed in the interfacial layer (Fig. 3(c) 0.42 min). The major peak at 710.4 eV corresponds to the Fe–O band for α-Fe_2O_3 or Fe_3O_4 [32], while the sub-peak at 707.0 eV evidences the existence of FeSi or $FeSi_2$ [30], although the content is low. Changes in the binding energy of O1s indicated the variation of oxides formation (Fig. 3(d)). In the surface Si-oxide layer (0.14 min), the oxygen atoms mainly exist in silicon oxides form or at interstices. As illustrated by the Si2p spectra, the O–Si bonding energy is different from that in thermally oxidized SiO_2 (3.08 min). In the interfacial layer (0.42 min), the O1s peak at 530.8 eV was broadened to a great extent, including a sub-peak character from O–Fe bonds in Fe_3O_4 at 530.7 eV [33], O–Fe band in α-Fe_2O_3 at 529.8 eV [34] and a sub-peak of O–Si bonds in SiO_2 at 533.0 eV [31].

The above analyses of the film microstructures and compositions indicate the major changes induced by ion-beam bombardment is the deformation in surface structure and the formation of oxides (including SiO_2, FeO, Fe_2O_3 and Fe_3O_4) at the interfaces. In the case of Si/Fe, only FeSi and $FeSi_2$ phases could be observed in the intermixing layer, since no or few oxygen atoms were engaged in the thin film deposition, as illustrated in Fig. 2. Pure Ar ion-beam bombardment during Si deposition only resulted in refinement of Fe grain size and changes in preferred orientations of ion silicide, as characterized by TEM (Fig. 1). However, a competition between oxygen, silicon, and iron to form oxides or silicides occurred with the O_2/Ar ion-beam bombardment. From the thermodynamic point of view, oxygen atoms prefer to form Fe_3O_4 instead of SiO_2, α-Fe_2O_3 and FeO, since Fe_3O_4 has more negative molar enthalpy of formation (−1116.7 kJ/mol) than SiO_2 (−850.8 kJ/mol), α-Fe_2O_3 (−830.5 kJ/mol) or FeO (−270.3 kJ/mol) [35,36]. As a result, the formation of Fe_3O_4 should dominate the initial stages of Si deposition with O_2/Ar ion-beam bombardment, while the content of FeSi and $FeSi_2$ is the lowest since it has the least negative molar enthalpy of formation (−73.85 kJ/mol and −78.62 kJ/mol, respectively) [37]. However, in the case of low oxygen content (8% O_2/Ar), the over-saturated Fe atoms tend to reduce the oxide to its lowest oxidation state [38], forming FeO at the interface. This FeO will be further oxidized to α-Fe_2O_3 with the increasing oxygen content in the ion beam. As the Si-oxide layer grows thicker, the Fe ions diffuse into the interfacial layer until they are consumed, and oxygen atoms react with Si instead to form silicon oxides. This resulted in the formation of top Si-oxide layer.

In order to investigate the influence of the above changes on the magnetic properties, hysteresis loops of the bilayer samples were measured at 298 K, 180 K and 10 K, shown in Fig. 4. At 298 K, most samples exhibited square hysteresis loops with more or less the same coercivity ($H_c \sim 1.25$ kA/m) (Fig. 4(a)). This indicated that capping and interfacial layers due to intermixing have little effect on the magnetization reversal of the Fe layer. However, the Si-oxide (8% O_2/Ar)/Fe bilayer presented a rounded hysteresis loop with smaller H_c ~477 A/m and lower remanence ($M_r/M_s \sim 0.4$). This reduction in squareness is a result of the changes in the domain wall rotation and reversal modes through interfacing with a different oxide (FeO instead of α-Fe_2O_3) created by the ion-beam bombardment. Broadened hysteresis loops were observed after field cooling at 10 K. This H_c enhancement at 10 K could be attributed to the exchange coupling between the ferromagnetic content Fe and the antiferromagnetic content α-Fe_2O_3 and FeO since the intermixed Fe-oxides layers underwent a magnetic phase transition from paramagnetic ($T \geqslant 180$ K due to finite size effects) to antiferromagnetic. However, since the relative amounts of α-Fe_2O_3 and FeO is low, only a very small (essentially unmeasurable) exchange bias field could be present. It is noted that there is a slight field loop shift to negative and positive in the Si-oxide (8% O_2/Ar)/Si and Si-oxide (21% O_2/Ar)/Si films, however, the origin of the shift is attributed to the remnant field from trapped flux in the superconducting solenoid.

The dependences of H_c on the temperature and oxygen/Ar ratio in the ion beam are shown in Fig. 5(a) and (b), respectively. The H_c of the unbombarded and Ar-ion-beam-bombarded Fe/Si bilayers exhibited slight increases after field cooling to 180 K (from 1.11 kA/m to 1.26 kA/m, and from 1.20 kA/m to 1.33 kA/m, respectively). This is likely due to a range of blocking temperatures caused by the size distribution of the Fe crystallites present [39]. The portion of the blocked particles increases with decreasing temperature, leading to enhanced H_c. However, the H_c of the unbombarded bilayer was reduced to 1.09 kA/m, and the H_c of

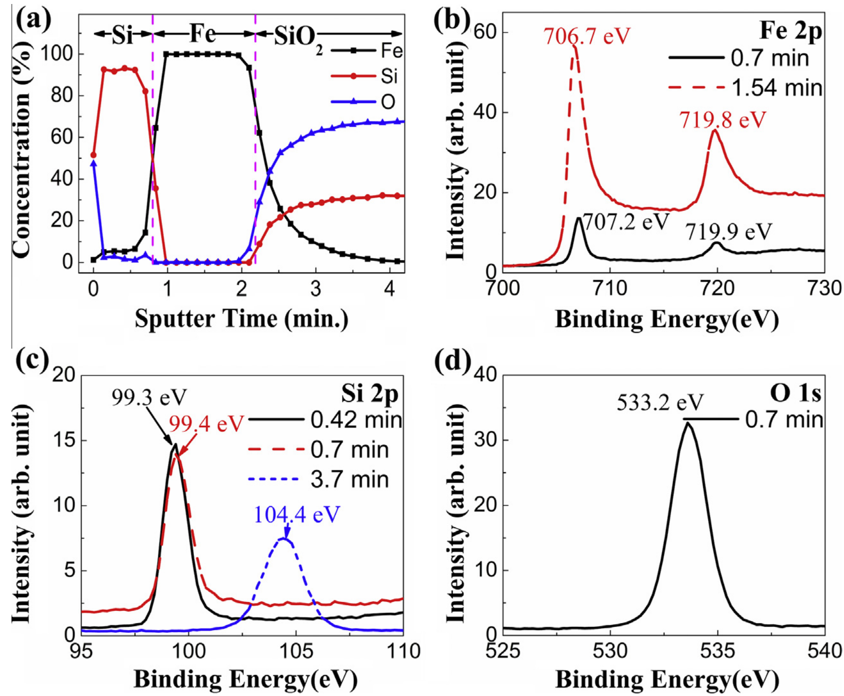

Fig. 2. The depth profiles of the chemical concentration of the un-bombarded Si/Fe bilayer measured by XPS (a), and the XPS spectra of Fe2p (b), Si2p (c), and O1s (d) after labeled sputter etching times.

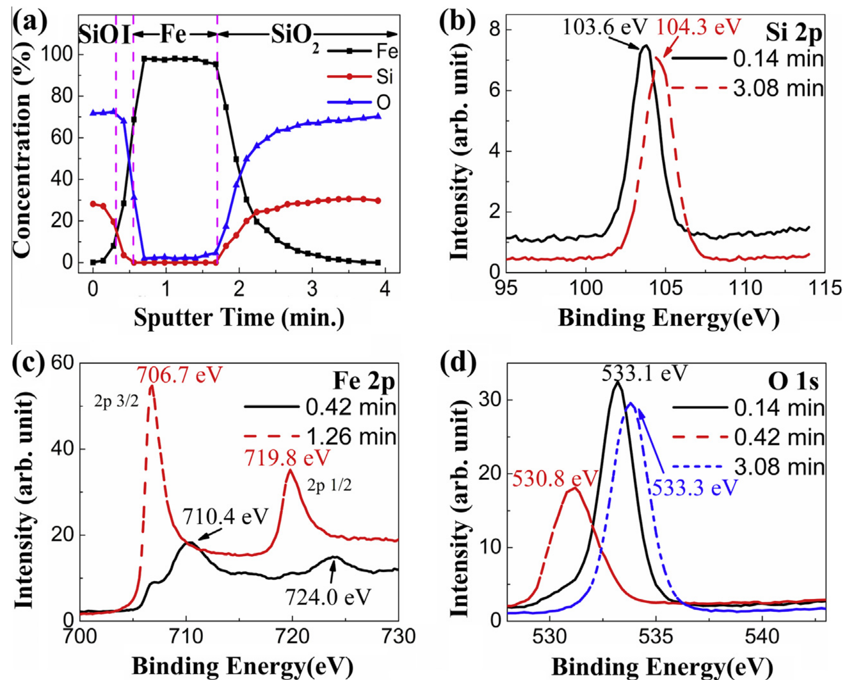

Fig. 3. The depth profiles of the chemical concentration in Si-oxide (41% O_2/Ar)/Fe bilayer measured by XPS (a), and the X-ray photoemission spectra of Fe2p (b), Si2p (c), and O1s (d).

Ar-ion-beam-bombarded bilayer was reduced to 1.07 kA/m after further field cooling to 10 K. This indicates that the samples may have entered a spin-glass-like phase (due to the structural and chemical disorder introduced by the bombardment) at low temperature, which resulted in this unusual temperature dependence of H_c (H_c increases with decreasing temperature, typically) [40]. On the other hand, the H_c of the films bombarded by the O_2/Ar ion beam mixtures increased gradually after field cooling to 180 K and 10 K. This is consistent with the gradual onset of exchange coupling between Fe and Fe-oxides below 180 K.

The H_c of the bilayers bombarded by ion beam with different O_2/Ar ratio are presented in Fig. 5(b) to further analyze the impact on the magnetism by ion-beam bombardment. Pure Ar^+ bombardment during Si deposition resulted in similar H_c to the un-bombarded Si/Fe bilayer and Ta/Fe bilayer ($H_c \sim 1.2$ kA/m, not shown). This indicated that the Fe anisotropy was not modified

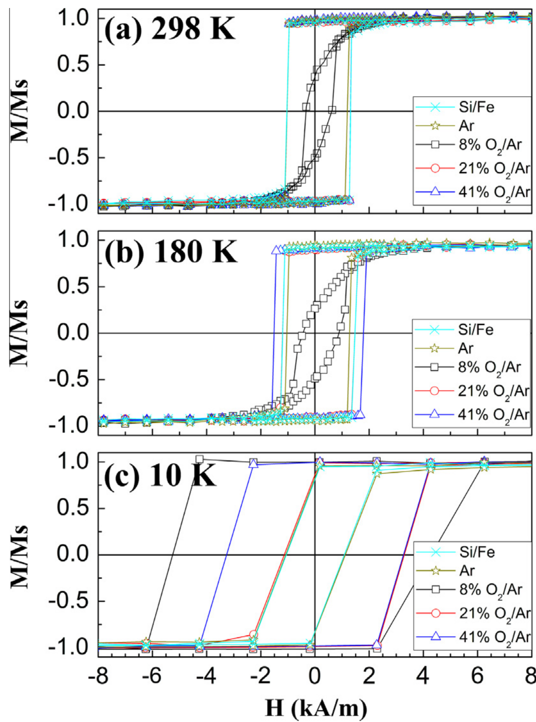

Fig. 4. The magnetic hysteresis loops of un-bombarded Si/Fe, Ar^+ plasma bombarded Si/Fe, Si-oxide (8% O_2/Ar)/Fe, Si-oxide (21% O_2/Ar)/Fe, and Si-oxide (41% O_2/Ar)/Fe bilayers measured at (a) 298 K, (b) 180 K and (c) 10 K after field cooling from 350 K.

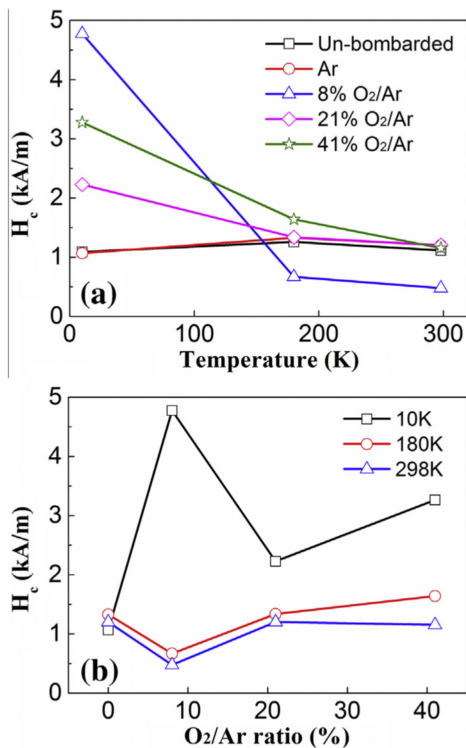

Fig. 5. The dependence of the coercivity (H_c) on the temperature (a) and O_2/Ar ratio in the ion beam (b).

by pure Ar ion-beam bombardment during Si-oxide layer deposition. The H_c of the Si-oxide (8% O_2/Ar)/Fe followed a different trend from other samples at all three temperatures. This is due to the different kind of oxide formed at the interface: it was FeO when bombarded by 8% O_2/Ar but it changed to Fe_2O_3 and Fe_3O_4 at 21% and 41% O_2/Ar as inferred from the SAED patterns. When measured at room temperature, the H_c of Si-oxide (8% O_2/Ar)/Fe was ~50% lower compared with that of the samples bombarded by pure Ar^+ ion beam. This reduction is likely the result of the reduced magnetocrystalline anisotropy of Fe layer due to the diffusion and implantation of oxygen atoms. Meanwhile, the H_c of Si-oxide (21% O_2/Ar)/Fe and Si-oxide (41% O_2/Ar)/Fe are almost the same as that of Si (Ar)/Fe (1.20 kA/m) at room temperature. These higher H_c compared with that of Si-oxide (8% O_2/Ar)/Fe is possibly due to the relatively higher surface anisotropy in Fe_2O_3/Fe compared with FeO/Fe. After field cooling to 180 K, the H_c of Si-oxide (21% O_2/Ar)/Fe and Si-oxide (41% O_2/Ar)/Fe film is slightly larger than that of Si (Ar)/Fe. This indicates that part of the Fe_2O_3 in the interface has started a phase transition to antiferromagnet, and weak exchange coupling between Fe and Fe_2O_3 was setting in. At 10 K, the Fe_2O_3 was fully transformed to antiferromagnetic, and more pronounced H_c enhancement was observed in Si-oxide (21% O_2/Ar)/Fe (2.23 kA/m) and Si-oxide (41% O_2/Ar)/Fe (3.26 kA/m). The stronger exchange coupling between FeO and Fe layer in Si-oxide (8% O_2/Ar)/Fe resulted in the largest H_c of 4.8 kA/m.

4. Conclusions

Si/Fe and Si-oxide/Fe bilayers were prepared by in-situ ion-beam bombardment with different O_2/Ar ratio during Si deposition, and their structural, compositional and magnetic properties were investigated and compared with those of the un-bombarded Si/Fe bilayer. A pure Ar^+ ion-beam altered the preferred orientations in Si, while the O_2/Ar ion beam changed the chemical composition of the samples by introducing an interfacial layer composed of oxides and silicides. The XPS measurements have identified FeSi and $FeSi_2$ in the Si/Fe interface. The Fe-oxides exhibited short-range order at the interfacial layer of Si-oxide/Fe, and changed from FeO to Fe_2O_3 as the oxygen content in the ion beam increased from 8% to 21% or higher, which is further evidenced in the measured SAED patterns. While the FeSi phase seemed to contribute little to the magnetic reversal of the Fe crystallite magnetizations, the Fe-oxides induced significant increases in H_c in the Si-oxide/Fe bilayers after field cooling to 10 K. The largest H_c (4.8 kA/m) was observed in the Si-oxide (8% O_2/Ar)/Fe at 10 K, which is believed to be from exchange coupling between Fe and the disordered FeO phase in the interface layer. Si-oxide (21% O_2/Ar)/Fe and Si-oxide (41% O_2/Ar)/Fe films exhibited comparatively lower H_c of 2.23 kA/m and 3.26 kA/m at 10 K, respectively, due to the different exchange coupling with the α-Fe_2O_3 phase present. Our results revealed that the microstructures and magnetic properties of Si-oxide/Fe bilayers could be tailored by the O_2/Ar ion-beam bombardment. The outcomes of this work will provide some guidance for considering the intermixing properties in spintronic devices using materials that have SiO_2/Fe interfaces.

Acknowledgements

This work was supported by MOST of Taiwan, FEB RAS of Russia, NSERC and CFI of Canada, Seed Funding Program for Basic Research and Small Project Funding Program from the University of Hong Kong, ITF Tier 3 funding (ITS/104/13, ITS/214/14), RGC-GRF Grant (HKU 704911P), and University Grants Committee of Hong Kong (Contract No. AoE/P-04/08).

References

[1] B.N. Engel, C.D. England, R.A. Van Leeuwen, M.H. Wiedmann, C.M. Falco, Phys. Rev. Lett. 67 (1991) 1910–1913.

[2] L.M. Falicov, D.T. Pierce, S.D. Bader, R. Gronsky, K.B. Hathaway, H.J. Hopster, D.N. Lambeth, S.S.P. Parkin, G. Prinz, M. Salamon, I.K. Schuller, R.H. Victora, J. Mater. Res. 5 (1990) 1299–1340.
[3] D.A. Steigerwald, I. Jacob, W.F. Egelhoff Jr, Surf. Sci. 202 (1988) 472–492.
[4] M. Maurer, J.C. Ousset, M.F. Ravet, M. Piecuch, Europhys. Lett. 9 (1989) 803.
[5] C.L. Fu, A.J. Freeman, Phys. Rev. B 35 (1987) 925–932.
[6] J.M. Florczak, E.D. Dahlberg, Phys. Rev. B 44 (1991) 9338–9347.
[7] S. Yuasa, T. Nagahama, A. Fukushima, Y. Suzuki, K. Ando, Nat. Mater. 3 (2004) 868–871.
[8] J. Alvarez, A.L. Vázquez de Parga, J.J. Hinarejos, J. de la Figuera, E.G. Michel, C. Ocal, R. Miranda, Phys. Rev. B 47 (1993) 16048–16051.
[9] R. Stephan, A. Mehdaoui, D. Berling, P. Wetzel, J. Appl. Phys. 105 (2009) 013919.
[10] R. Stephan, A. Mehdaoui, F. Ott, P. Wetzel, J. Magn. Magn. Mater. 320 (2008) 3378–3383.
[11] R. Kläsges, C. Carbone, W. Eberhardt, C. Pampuch, O. Rader, T. Kachel, W. Gudat, Phys. Rev. B 56 (1997) 10801–10804.
[12] G.J. Strijkers, J.T. Kohlhepp, H.J.M. Swagten, W.J.M.d. Jonge, Phys. Rev. B 60 (1999) 9583–9587.
[13] G. Principi, P. Polato, A. Paccagnella, A. Maddalena, S.L. Russo, G. Battaglin, Hyperfine Interact. 46 (1989) 517–526.
[14] X. Lin, A.S. Murthy, G.C. Hadjipanayis, C. Swann, S.I. Shah, J. Appl. Phys. 76 (1994) 6543–6545.
[15] S. Couet, K. Schlage, R. Rüffer, S. Stankov, T. Diederich, B. Laenens, R. Röhlsberger, Phys. Rev. Lett. 103 (2009) 097201.
[16] J.A. Christodoulides, N.B. Shevchenko, G.C. Hadjipanayis, V. Papaefthymiou, J. Appl. Phys. 81 (1997) 5558–5560.
[17] K.W. Lin, M. Mirza, C. Shueh, H.R. Huang, H.F. Hsu, J. van Lierop, Appl. Phys. Lett. 100 (2012) 122409.
[18] S.N. Okuno, S. Hashimoto, K. Inomata, J. Appl. Phys. 71 (1992) 5926–5929.
[19] X. Li, K.W. Lin, H.Y. Liu, D.H. Wei, G.J. Li, P.W.T. Pong, Thin Solid Films 570 (2014) 383.
[20] K.W. Lin, R.J. Gambino, L.H. Lewis, J. Appl. Phys. 93 (2003) 6590–6592.
[21] G. Li, C.W. Leung, C. Shueh, H.-F. Hsu, H.-R. Huang, K.-W. Lin, P.T. Lai, P.W.T. Pong, Surf. Coat. Technol. 228 (2013) S437–S441.
[22] K.W. Lin, P.H. Ko, Z.Y. Guo, H. Ouyang, J. van Lierop, J. Nanosci. Nanotechnol. 7 (2007) 265–271.
[23] S.B. Ogale, R. Joshee, V.P. Godbole, S.M. Kanetkar, V.G. Bhide, J. Appl. Phys. 57 (1985) 2915.
[24] M. Milosavljević, S. Dhar, P. Schaaf, N. Bibić, Y.-L. Huang, M. Seibt, K.P. Lieb, J. Appl. Phys. 90 (2001) 4474–4484.
[25] S.K. Sinha, D.C. Kothari, T. Som, V.N. Kulkarni, K.G.M. Nair, M. Natali, Nucl. Instr. Meth. B 170 (2000) 120.
[26] G. Principi, P.Q. Zhang, G. Battaglin, S. Lo Russo, A. Paccagnella, J. Mater. Sci. Lett. 7 (1988) 484.
[27] K.W. Lin, F.T. Lin, Y.M. Tzeng, Z.Y. Guo, Eur. Phys. J. B 45 (2005) 237.
[28] W.M. Lau, I. Bello, L.J. Huang, X. Feng, M. Vos, I.V. Mitchell, J. Appl. Phys. 74 (1993) 7101–7106.
[29] C.D. Wagner, W.M. Riggs, L.E. Davis, J. Moulder, Handbook of X-ray Photoelectron Spectroscopy, first ed., Perkin Elmer Corporation, 1979.
[30] V. Kinsinger, I. Dezsi, P. Steiner, G. Langouche, J. Phys.: Condens. Matter 2 (1990) 4955–4961.
[31] E.J. Paparazzo, J. Electron Spectrosc. Relat. Phenom. 43 (1987) 97–112.
[32] M. Oku, K. Hirokawa, J. Electron Spectrosc. Relat. Phenom. 8 (1976) 475–481.
[33] P. Marcus, J.M. Grimal, Corros. Sci. 33 (1992) 805–814.
[34] N.S. McIntyre, D.G. Zetaruk, Anal. Chem. 49 (1977) 846–851.
[35] T. Akira, I. Akihisa, Mater. Trans. – JIM 41 (2000) 1372–1378.
[36] M.E. Huntelaar, E.H.P. Cordfunke, W. Ouweltjes, J. Chem. Thermodyn. 24 (1992) 139–143.
[37] J. Acker, K. Bohmhammel, G.J.K. van den Berg, J.C. van Miltenburg, C. Kloc, J. Chem. Thermodyn. 31 (1999) 1523–1536.
[38] S. Couet, K. Schlage, K. Saksl, R. Röhlsberger, Phys. Rev. Lett. 101 (2008) 056101.
[39] P. Vavassori, E. Angeli, D. Bisero, F. Spizzo, F. Ronconi, Appl. Phys. Lett. 79 (2001) 2225–2227.
[40] Q.-L. Ye, C.-M. Feng, X.-J. Xu, J.-S. Jin, A.-G. Xia, G.-X. Ye, J. Appl. Phys. 98 (2005) 013906.